

Parametric Instability Growth Rates of Progressive Mode-1 Internal Wave

Philippe Odier¹, James Munroe², Sylvain Joubaud¹, Thierry Dauxois¹

¹Laboratoire de Physique,
École Normale Supérieure de Lyon
46, allée d'Italie, 69364 Lyon Cedex 07, France
podier@ens-lyon.fr

²Department of Physics and Physical Oceanography
Memorial University of Newfoundland
St. John's, NL A1B 3X7, Canada

Abstract

Internal waves are known to be inherently unstable and evolve in time by transferring energy to different length and time scales. While there has been substantial work investigating internal waves stability theoretically and numerically, there has been comparatively few laboratory studies examining these instabilities. Using a full-depth wave generator to force a vertical mode-1 wave in a narrow rectangular tank, we observe the evolution of the wave field. The fluid motion is quantitatively measured using synthetic schlieren. We present preliminary results regarding the growth rates of secondary waves due to parametric sub-harmonic instability.

1 Introduction

Internal gravity waves can spontaneously become unstable, producing waves of smaller frequency and larger wavelength. The history of this problem has been explored in a review article by [Staquet and Sommeria \(2002\)](#) considering both propagating and standing waves. This instability represents an interesting phenomenon in oceanic situations, since it provides a good way to transfer energy from large scale waves to smaller scales, where it can be dissipated, without the need of a turbulent cascade.

[Thorpe \(1968\)](#) performed experiments in a rectangular container using plungers on the sides to drive low-order standing modes. For large amplitude forcing, ‘irregularities’ were observed that led to mixing and overturning. A series of experiments were performed by [McEwan and collaborators](#) to investigate parametric instability. [McEwan \(1971\)](#) performed experiments with an oscillating paddle in a linearly stratified fluid. He observed the formation of ‘traumata’ or sharp density discontinuities that were linked to growth of secondary waves by parametric instability. [Orlanski \(1972\)](#) considered standing internal gravity waves examining especially how large amplitude waves broke for low frequency forcing. Laboratory experiments by [Benielli and Sommeria \(1998\)](#) demonstrated parametric subharmonic instability qualitatively. They applied a varying body force to parametrically excite a primary standing wave. Secondary waves due to parametric sub-harmonic instability were observed to sporadically grow and break.

We report here on experiments performed with a wave generator that produces sinusoidal vertical waves propagating along a rectangular tank. We quantitatively measure the growth rate of the instability. As will be pointed out in the discussion, these results are preliminary, and therefore no comparison to theoretical predictions can yet be made. In addition, the dependence of the measured growth rates on various control parameters still has to be studied in more details.

2 Internal waves and Parametric Subharmonic Instability

Internal waves result from the balance of inertia of a fluid parcel and a restoring buoyancy force in a stratified fluid. This buoyancy force is characterized by the buoyancy frequency, N . The 2-D Boussinesq inviscid equations of motion corresponding to conservation of momentum and mass can be written as

$$\frac{\partial^2 \nabla^2 \psi}{\partial t^2} + N^2 \frac{\partial^2 \psi}{\partial x^2} = -\frac{\partial}{\partial t} J(\nabla^2 \psi, \psi) - \frac{\partial}{\partial x} J(\rho', \psi). \quad (1)$$

Since the flow is assumed to be incompressible, we use a stream function ψ to represent velocity $\vec{u} = (u, v) = (\partial\psi/\partial z, -\partial\psi/\partial x)$ and ρ' represents the perturbation density field.

Upon linearization, the right side of the equation of motion is zero which leads to the usual dispersion relation for frequency ω

$$\omega^2 = N^2 \left(1 - \frac{k_z^2}{k^2} \right) \quad (2)$$

where k and k_z are respectively the modulus and the vertical component of the wave number, \vec{k} . For small amplitudes, it can be assumed that several waves could concurrently exist simply as a linear superposition. However, in the case of a resonant triad interaction, where three waves verify a condition of spatial resonance

$$\vec{k}_0 + \vec{k}_1 + \vec{k}_2 = 0 \quad (3)$$

and a condition of temporal resonance

$$\omega_0 + \omega_1 + \omega_2 = 0, \quad (4)$$

the non-linear terms act as forcing terms transferring energy between the three waves. In particular, a finite amplitude, larger length scale, higher frequency wave can transfer energy to produce two secondary waves of smaller length scales and lower frequencies.

It has been shown by [Hasselmann \(1967\)](#) that growth of secondary waves occurs only if $|\omega_1| + |\omega_2| = |\omega_0|$. The difference triads, where $||\omega_1| - |\omega_2|| = |\omega_0|$, are only neutrally stable. In the case of large scale waves, such as can be observed in the ocean, where the dissipation is weak, it appears that the maximum growth rate of the instability occurs for perturbations of half the primary wave frequency $\omega_1 \simeq \omega_2 \simeq \omega_0/2$, in the limit of high wavenumbers $||\vec{k}_1|| \simeq ||\vec{k}_2|| \gg ||\vec{k}_0||$. The instability then takes the form of a parametric instability, and is thus called ‘‘Parametric Subharmonic Instability’’ (PSI). In the case of waves in an experimental tank, this particular condition is not fulfilled, but by extension, we will still call PSI the observed phenomenon, since the corresponding physical mechanism is the same.

3 Method and Analysis

3.1 Experimental setup

Internal waves can be generated in a laboratory setting by a variety of means using an oscillating cylinder ([Mowbray and Rarity \(1967\)](#)), flow over topography, plungers ([Thorpe \(1968\)](#)) or an oscillating paddle ([McEwan \(1971\)](#)). To generate monochromatic vertical modes, we chose a relatively new way using a set of oscillating plates ([Gostiaux et al.](#)

(2007); Mercier et al. (2010)). The vertical wave number is fixed by the relative horizontal offsets of the plates. The frequency of the waves is controlled by the rotation rate of the motor which in turn is linearly dependent on the voltage applied to the motor.

The tank is filled with a linear salt water stratification using the standard double bucket technique (Oster (1965)). The stratification is roughly $N = 1 \text{ rad} \cdot \text{s}^{-1}$ for most experiments. It is measured using a conductivity probe from Precision Measurement Engineering which is calibrated using reference solutions whose density is measured with a Anton Paar 35N density meter. The conductivity probe is traversed vertically through the water before an experiment begins, using a computer controlled lead screw. A linear best fit line is made to the measured density profile, the slope of which is used to define a buoyancy frequency for the experiment. There is typically some mixing (1-3 cm) at the top and bottom of the tank due to the filling procedure. The best fit line is estimated on the interior of the profile. The stratification is measured at the beginning of the day before any experiments are performed.

An Allied Vision StingRay 146B camera is used to acquire images at a rate of 1.875 frames per second. The camera is positioned roughly 2 m in front of the tank. Typical experiments last for about 10 minutes to capture approximately a hundred buoyancy periods of evolution of the wave field. The maximum camera resolution is 1280x960 which for our choice of zoom leads to a scaling of approximately 0.04 cm per pixel. The tank is illuminated with a light sheet from behind with a random pattern of dots.

We define a lab reference frame for the experiments where the origin is the lower left corner inside the tank at the equilibrium position of the right edge of the plates. See figure 1 for a schematic. Various experiments were performed with varying forcing frequency.

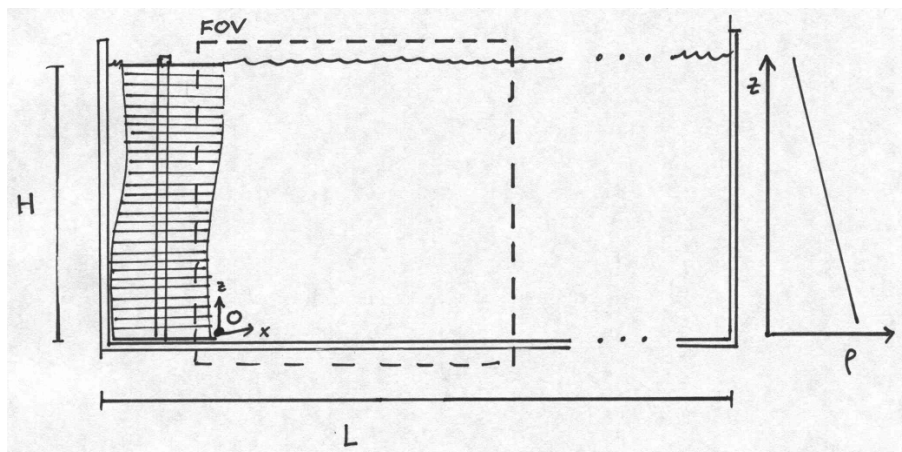


Figure 1: Setup of experiment. Plates of wave generator on the left force the linear stratified fluid inside the tank of length $L = 80 \text{ cm}$ and depth $H = 32 \text{ cm}$. The camera sees only a limited field of view (marked as FOV) of the entire apparatus. The origin, marked by O , is positioned inside the tank at the bottom, at the equilibrium position of the plates.

3.2 Image analysis

The motion of the fluid is inferred by synthetic schlieren (Dalziel et al. (2000)) using the method of pattern matching refractometry. This optical method takes advantage of the linear dependence of the index of refraction on the density of the fluid. Internal waves

perturb the local density field and produce an optical distortion of a pattern behind the tank which appears as a localized displacement of the background pattern. We can relate this apparent displacement back to actual movement of the stratified fluid. The technique assumes the flow is uniform across the tank. The synthetic schlieren method estimates the $\partial\rho'/\partial x$ and $\partial\rho'/\partial z$ fields.

The apparent motion of the dots in the background pattern is computed using a cross-correlation algorithm implemented in the CIVx software suite (Fincham and Delerce (2000)). The cross-correlation is performed between an initial image taken before the experiment starts and the system is at rest and a later image taken during the experiment. Since the experiment is recorded over many frames, this cross-correlation routine is repeated giving the apparent displacements of the dots as a function of time. The displacement, given in coordinates of the lab reference frame, is decomposed into both horizontal, Δx , and vertical, Δz , components. The cross-correlation algorithm takes as parameters the size of an interrogation box, i_b , and a search area, i_s . Both of these boxes are squares with values of $i_b = 21$ pixels and $i_s = 31$ pixels. The interrogation boxes are spaced with a resolution in Δx and Δz of 20 pixels. The measurements are performed on a rectangular grid over the interior of the tank and the time resolution is given by the frame rate of the acquisition system.

3.3 Spectral filtering

At each spatial position, a time series of each density gradient $\partial\rho'/\partial x$ and $\partial\rho'/\partial z$ can be considered. The power spectrum obtained using a Fourier transform identifies the dominant frequencies in that time series. A spatial average of each of these spectra identifies the dominant frequencies in the overall fluid motion. The distinct peaks in this averaged spectrum are identified and recorded.

A signal with multiple discrete frequency components can be decomposed using amplitude demodulation. The result of this operation applied to both density gradients decomposes them into multiple components of known frequency. Applying the superposition principle by subtracting off these known components from the original signal leaves a continuous spectrum. The relative fraction of the energy of this remaining signal to the original signal gives a measurement of what fraction of the signal has been explained by the multiple discrete frequency decomposition.

The amplitude as a function of time of each component is determined. The amplitude is estimated as the spatial maximum. On a semi-log plot, assuming that a straight line segment of the amplitude function can be identified, a linear regression applied to this segment gives the growth rate λ .

4 Results

Figure 2 shows an experiment with $\omega/N = 0.9$. At early times a clean mode-1 vertical wave is seen propagating to the right away from the wave generator. At later times, there are waves of multiple vertical wave number in the field of view.

The spectrum of the example signals from figure 2 are shown in figure 3, with frequency normalized by the buoyancy frequency. The plot displays two curves corresponding to the spectrum computed with either the vertical displacement, or the horizontal displacement. The largest peak on the right side of the spectrum corresponds to the forcing frequency, ω_0 . To the left of this forcing frequency, a pair of spectral peaks are observed. If this pair of

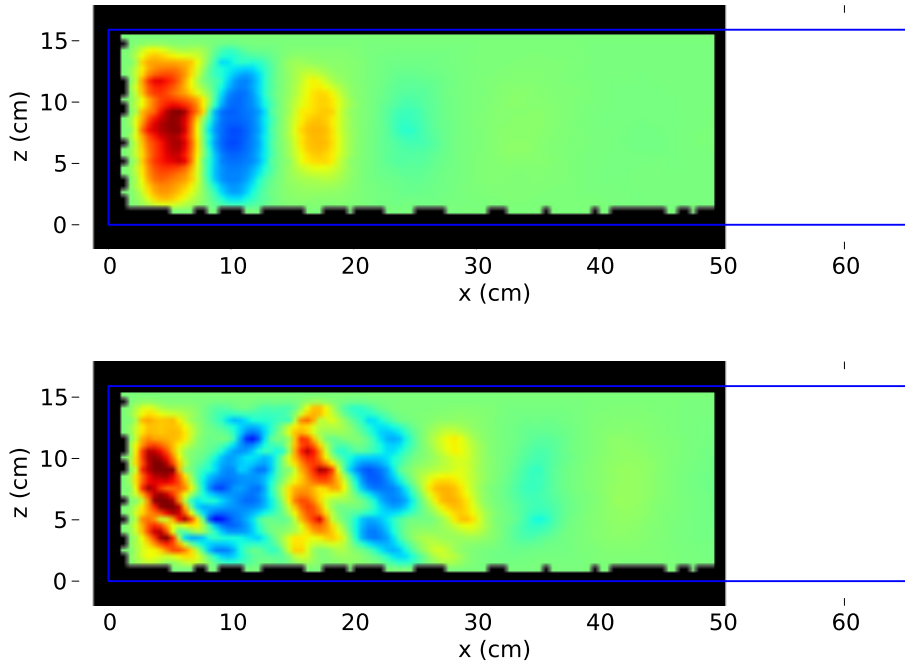


Figure 2: $d\rho/dx$ at early and late times ($t = 9.8T$ and $t = 19.9T$). The blue box indicates the extension of the tank from the edge of the plates to its end-wall.

clearly defined peaks verifies the relationship $\omega_0 = \omega_1 + \omega_2$, it is interpreted as evidence of parametric instability. There is also a background level of noise over a broad frequency range. The strong peak near $\omega/N = 0$ corresponds to slow changes (relative to the buoyancy period) of the relative frequency content of the wave field.

Once each spectral component is identified, it is isolated by filtering, as explained in the previous section, and its amplitude is computed. Figure 4 shows an example of computed amplitude versus time (scaled by the buoyancy period T_{BV}), for the 3 frequencies identified in a case of PSI. The amplitude of the primary wave (top plot), after an initial transient, stays fairly constant, until the secondary waves reach their maximum amplitude. Then it decreases slightly. This is a clear signature that energy is transferred from the large scale primary wave to smaller scale secondary waves.

The secondary waves (middle and bottom plots) start to grow after a few buoyancy periods and the linear increase of their amplitude in this semi-log representation confirms an exponential growth. The slope of this linear increase, computed by a best line fit, gives a direct measurement of the growth rate, scaled by the buoyancy period.

Figure 5 shows a summary of the growth rates measured for different forcing frequencies. The various colors correspond to different realizations of the stratified tank, showing that there is a variability in the growth rate, depending of the exact details of the stratification. However, there is a clear trend showing that below a threshold in forcing frequency, around 0.9 times the buoyancy frequency, PSI does not develop. Then, above the threshold, the growth rates increase, to reach about a quarter of the buoyancy period when the forcing frequency is close to the Brunt-Väisälä frequency.

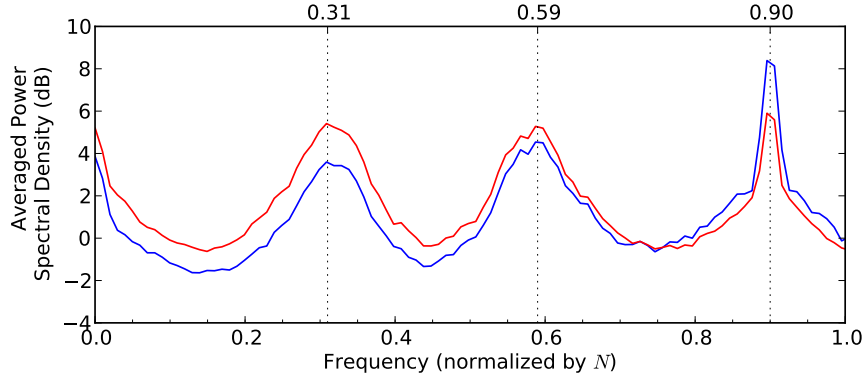


Figure 3: Spectrum showing primary wave and lower frequency secondary waves. Red line, vertical motion. Blue line, horizontal motion.

5 Conclusion and discussion

Using a high resolution method of synthetic schlieren, coupled with a Fourier analysis allowing us to separate the time dependence of the frequency components of a set of internal waves, we were able to measure the growth rate of the instability produced by resonant triad interactions between internal waves. Since these results are only preliminary, a number of effects remain to be studied and understood:

- The particular structure of the stratification appears to be very important in the outcome of these experiments. All stratification tests are nominally linear. However, there is always some amount of either surface or bottom mixing (or both), which occurs during the filling of the tank, during successive experiments, or over time due to surface heating and cooling. Experiments performed on successive days with the same stratification (that is, same value of N in the middle part of the tank) but different amounts of mixing at the top and the bottom produce very different evolutions of the secondary waves with the same external forcing. We must conclude that small scale details of the stratification are important in predicting the growth of secondary waves due to parametric instability.
- The next step of this analysis will be to compare the measured growth rates to theoretical predictions. However, the amplitude of the primary wave is a critical parameter in determining the theoretical growth rate. And as we have pointed out, this amplitude is not independent of the secondary wave growth. Therefore, particular attention has to be paid to how this amplitude will be determined.
- For experiments with high forcing frequency, the horizontal group velocity of the primary wave is very small. That is, the time it takes for linear mode-1 waves to propagate to the end of the tank and return to the measurement area is longer than the duration of the experiment. But in the case of lower forcing frequency, the primary wave can reflect off the end wall and come back faster. It is then very likely that the primary wave will establish a standing wave. The amplitude of the standing wave is obviously not the same as the amplitude of the forcing. Since growth rate is dependent on the amplitude of the primary wave, application of the theory is somewhat complicated by the fact that, in this case of low forcing frequency, the primary wave amplitude is function of the length of the tank.

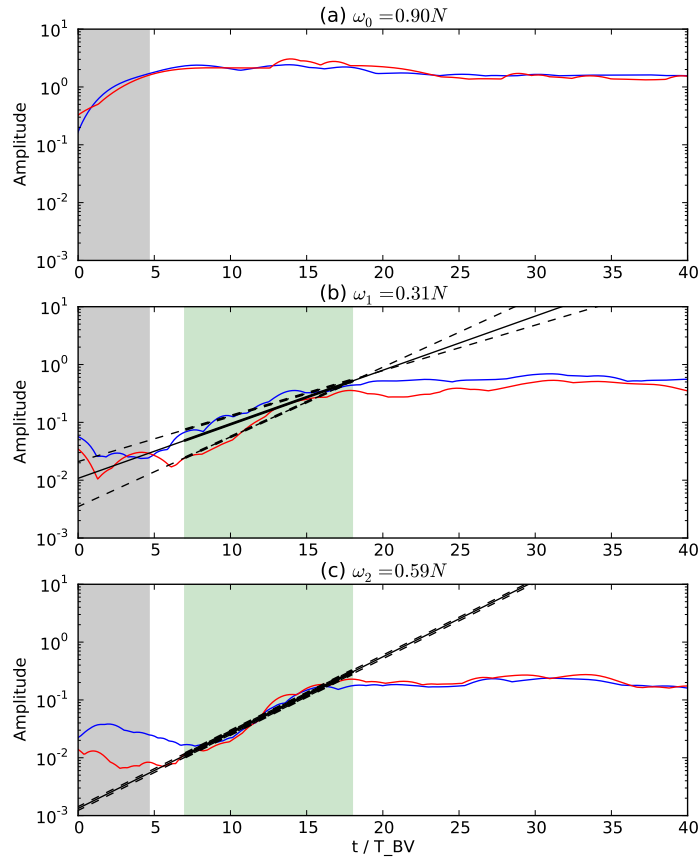


Figure 4: Amplitude of the 3 frequency components (top, primary wave, middle and bottom, secondary waves) as function of time. As in the previous figure, red line represents vertical motion, blue line, horizontal motion. The dashed lines represent the linear fits of each components, the solid line is the average of both dashed lines.

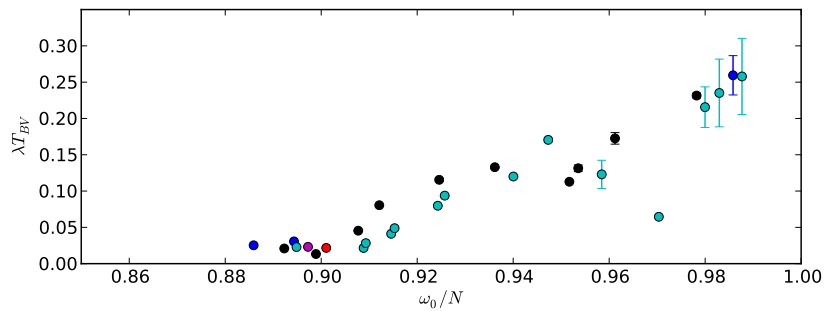


Figure 5: Growth rates as a function of ω/N . The color of the dots correspond to different days, therefore slightly different stratifications.

To extend this project further, we might study the spatial dependence on wave growth. In particular, we could test a prediction by [Koudella and Staquet \(2006\)](#), stating that the PSI most likely grows in regions where negative vorticity of the primary wave coincides with positive vertical density gradient due to this wave. We also want to investigate the evolution of other forced waves, namely, plane waves or wave beams (Thomas-Stevenson profile). In addition, by running this experiment in a rotating frame of reference, we can explore the effect of rotation on the evolution of the internal waves. In such a rotating frame, the lower cut-off for internal waves is the Coriolis frequency. We could then test the effect of a “critical latitude”. For simplicity, we have used a linear stratification. Other possibilities include an exponential profile or more general (realistic) stratification profiles. Furthermore, we have only considered two-dimensional forcing: with a modification of the wave generator and the tank, we could explore three-dimensional modes.

References

- Benielli, D. and Sommeria, J. (1998). Excitation and breaking of internal gravity waves by parametric instability. *J. Fluid Mech.*, pages 117–144.
- Dalziel, S., Hughes, G. O., and Sutherland, B. (2000). Whole-field density measurements by ‘synthetic schlieren’. *Exp. Fluids*, 28:322–335.
- Fincham, A. and Delerce, G. (2000). Advanced optimization of correlation imaging velocimetry algorithms. *Exp. Fluids*, 29(7):S013—S022.
- Gostiaux, L., Didelle, H., Mercier, S., and Dauxois, T. (2007). A novel internal waves generator. *Exp. Fluids*, 42(1):123–130.
- Hasselmann, K. (1967). A criterion for nonlinear wave stability. *J. Fluid Mech.*, 30(04):737.
- Koudella, C. and Staquet, C. (2006). Instability mechanisms of a two-dimensional progressive internal gravity wave. *J. Fluid Mech.*, 548:165–196.
- McEwan, A. (1971). Degeneration of resonantly-excited standing internal gravity waves. *J. Fluid Mech.*, 50(03):431–448.
- Mercier, M., Martinand, D., Manikandan, M., Gostiaux, L., Peacock, T., and Dauxois, T. (2010). New wave generation. *J. Fluid Mech.*, 657:308–334.
- Mowbray, D. and Rarity, B. (1967). A theoretical and experimental investigation of the phase configuration of internal waves of small amplitude in a density stratified liquid. *J. Fluid Mech.*, 28:1–16.
- Orlanski, I. (1972). On the breaking of standing internal gravity waves. *J. Fluid Mech.*, 54(04):577–598.
- Oster, G. (1965). Density gradients. *Sci. Am.*, 213.
- Staquet, C. and Sommeria, J. (2002). Internal gravity waves: From instabilities to turbulence. *Ann. Rev. Fluid Mech.*, 34:559–593.
- Thorpe, S. (1968). On standing internal gravity waves of finite amplitude. *J. Fluid Mech.*, 32(Part 3):489–528.